Government of **Western Australia**
Department of **Mines and Petroleum**

RECORD 2013/3

HYLOGGER-3: IMPLICATIONS OF ADDING THERMAL-INFRARED SENSING

by
EA Hancock, AA Green, JF Huntington, MC Schodlok and LB Whitbourn




Geological Survey of Western Australia

Government of **Western Australia**
Department of **Mines and Petroleum**

Record 2013/3

HYLOGGER-3: IMPLICATIONS OF ADDING THERMAL-INFRARED SENSING

by
EA Hancock, AA Green[1], JF Huntington[1], MC Schodlok[1] and LB Whitbourn[1]

1 CSIRO Earth Science and Resource Engineering, PO Box 136, North Ryde, Sydney, NSW 1670

Perth 2013

Geological Survey of Western Australia

MINISTER FOR MINES AND PETROLEUM
Hon. Bill Marmion MLA

DIRECTOR GENERAL, DEPARTMENT OF MINES AND PETROLEUM
Richard Sellers

EXECUTIVE DIRECTOR, GEOLOGICAL SURVEY OF WESTERN AUSTRALIA
Rick Rogerson

REFERENCE
The recommended reference for this publication is:
Hancock, EA, Green, AA, Huntington, JF, Schodlok, MC and Whitbourn, LB 2013, HyLogger-3: Implications of adding thermal-infrared sensing: Geological Survey of Western Australia, Record 2013/3, 24p.

National Library of Australia Card Number and ISBN 978-1-74168-525-1

Grid references in this publication refer to the Geocentric Datum of Australia 1994 (GDA94). Locations mentioned in the text are referenced using Map Grid Australia (MGA) coordinates, Zone 50. All locations are quoted to at least the nearest 100 m.

Published 2013 by Geological Survey of Western Australia
This Record is published in digital format (PDF) and is available online at <www.dmp.wa.gov.au/GSWApublications>.

Further details of geological products and maps produced by the Geological Survey of Western Australia are available from:
Information Centre
Department of Mines and Petroleum
100 Plain Street
EAST PERTH WESTERN AUSTRALIA 6004
Telephone: +61 8 9222 3459 Facsimile: +61 8 9222 3444
www.dmp.wa.gov.au/GSWApublications

Contents

Figures

Tables

HyLogger-3: Implications of adding thermal-infrared sensing

by

EA Hancock, AA Green[1], JF Huntington[1], MC Schodlok[1] and LB Whitbourn[1]

Abstract

The HyLogger technology comprises a suite of core- and chip-logging, and spectroscopic-imaging systems developed by the CSIRO Minerals Down Under Flagship. In 2011 the seven second-generation HyLogger-2 instruments deployed to Australian State and Territory Geological Surveys as part of the AuScope National Virtual Core Library (NVCL) program were upgraded with new thermal-infrared (TIR) sensors to create the HyLogger-3 generation of instruments. The spectral range of the TIR spectrometer is 6000–14 500 nm, the bandwidth where anhydrous silicates show diagnostic spectral signatures related to fundamental molecular vibrations. The HyLogger-3 system is potentially capable of detecting common rock-forming minerals (feldspar, quartz, pyroxene, garnet, olivine, carbonate, and phosphate), as well as a number of hydroxyl-bearing minerals that are also measurable at visible near-infrared (VNIR, 380–1000 nm) and shortwave-infrared (SWIR, 1000–2500 nm) wavelengths.

Since the installation of the NVCL HyLogger-2 in the Perth Core Library, the Geological Survey of Western Australia (GSWA) has scanned more than 70 000 m of core from 270 mineral and petroleum drillholes from July 2009 to April 2013, including about 44 000 m of core logged with a HyLogger-3.

Complexities with TIR data acquisition and interpretation include temperature control, light scattering from the surface of core, spectral mixing and non-uniqueness of mineral spectra, and influence of crystallographic orientation of rock-forming grains. However, new analysis techniques and more expansive mineral reference libraries have greatly improved our capacity to identify rock-forming and alteration minerals in logged drillcore, enabling, for example, better differentiation of igneous rock types based on their feldspar composition. The TIR information also assists in interpretation of the VNIR–SWIR mineralogy data.

In this study we demonstrate how TIR data from the Minnie Springs molybdenum–copper–tungsten (Mo–Cu–W) prospect in the Gascoyne Province, and the Cummins Range rare earth elements (REE) prospect in the Kimberley Craton can be used to identify important rock-forming, ore-hosting and alteration mineral assemblages, and vectors to mineralization.

KEYWORDS: core logging, core sampling, drill core, mineral alteration, thermal-infrared imagery, thermal-infrared scanning

1 CSIRO Earth Science and Resource Engineering, PO Box 136, North Ryde, Sydney, NSW 1670

Introduction

The aim of this Record is to introduce to HyLogging users the basic physical processes involved in acquiring quality thermal-infrared (TIR) spectra, their characteristics, benefits and uncertainties in data interpretation. Our experience indicates that the new TIR data can be applied to many geological and mineralogical problems. Examples are illustrated here using data from Minnie Springs Mo–Cu–W and Cummins Range REE mineralization.

This Record complements GSWA Record 2010/17 The GSWA NVCL HyLogger: rapid mineralogical analysis for characterizing mineral and petroleum core (Hancock and Huntington, 2010).

Sinve the NVCL HyLogger-2 was installed in the Perth Core Library, GSWA has scanned more than 70 000 m of core from 270 mineral and petroleum drillholes from July 2009 to April 2013 (Appendix 1). Analysed core is part of the GSWA historical collection. New core also arrives from exploration and mining sites. Processed and interpreted hyperspectral data have been used to support research projects undertaken by GSWA mapping geologists, mineral and petroleum systems geoscientists, academic researchers and students, and mineral exploration and petroleum companies.

One of the major sources of drillcore for scanning by the GSWA HyLogger is the Western Australian Government's Exploration Incentive Scheme (EIS) Co-funded Drilling Program. All diamond drillcore delivered to the Perth or Kalgoorlie Core Libraries is routinely scanned by the HyLogger. Processed data are provided to in-house and corporate clients as graphic images, spreadsheets, and The Spectral Geologist (TSG) software files.

Processed spectral data, mineralogy, and high-resolution core images are also being progressively uploaded to a web service on the AuScope Portal that is accessible worldwide for researchers and industry at <portal.auscope.org/portal/gmap.html>.

The HyLogger-3 thermal-infrared system

The first airborne multispectral TIR imaging systems for geological applications were developed by the National Aeronautics and Space Administration (NASA) in the 1980s. The launch of the ASTER (Advanced Spaceborne Thermal Emission and Reflection Radiometer) satellite system followed in 1999. A field portable Fourier transform infrared (FTIR) system and the first airborne hyperspectral TIR system were subsequently launched. In the 2000s, CSIRO developed a TIR drillcore logging system, the TIR HyLogger (Cudahy et al., 2009), which was used in 2004–05 to expand the spectral bandwidth of the HyLogger-1 system in the Joe Lord Core Library in Kalgoorlie (Huntington et al, 2008). In 2011, the seven, second-generation HyLogger-2 instruments deployed to Australian State and Territory Geological Surveys of the AuScope National Virtual Core Library (NVCL) program were upgraded with new TIR sensors to create the HyLogger-3 generation of instruments.

HyLogger-2 instruments measure mineral information based on their spectroscopic features in the visible (VNIR, 380–1000 nm) and shortwave-infrared (SWIR, 1000–2500 nm) range, principally iron oxides, sulphates, and OH-bearing minerals (<speclab.cr.usgs.gov>; Hancock and Huntington, 2010). The spectral range of the new TIR spectrometer (6000–14 500 nm) covers a region where minerals have fundamental molecular vibrations and enables the measurement of diagnostic mineral spectral signatures associated with, for example, anhydrous silicates (feldspar, quartz, pyroxene, garnet, and olivine). The upgraded, extended spectrum (VNIR+SWIR+TIR) of the HyLogger-3 systems therefore allows the mapping of a much greater range of minerals (Table 1).

Thermal-infrared system hardware

The TIR spectrometer is based on a rapid-scan Fourier transform infrared (FTIR) sensor similar to that used for SWIR wavelengths (Huntington et al., 2008). It uses a rotating optical path length modulator to produce 12 spectral scans per second with a nominal spatial resolution of 10 mm square. In conjunction with a table scanning rate of 48 mm per second (Table 2), it delivers one spectral measurement for every 4 mm of travel. The spectral resolution in the wavelength domain varies continuously from 25 nm at 6000 nm to about 140 nm at 14 500 nm. The viewing location of the new TIR spectrometer telescope is 200 mm on side from the VNIR and SWIR telescopes, but data are synchronized using software.

The TIR spectrometer uses a liquid nitrogen-cooled mercury-cadmium-telluride (HgCdTe) photoconductive detector to measure bidirectional reflectance from drillcore irradiated by two focused blackbody sources at temperatures of approximately 700° C (Fig. 1). The background radiation is sampled at the beginning of each core tray by reflecting the ambient radiation into the detector using an aluminium mirror mounted on the X/Y table (background radiation inside a closed room with constant temperature has a blackbody spectrum). At the same time the transfer standard is sampled. This standard is calibrated to a diffuse reflecting gold standard housed in the TIR calibration unit that is measured every morning. The calibration unit incorporates hot and cold blackbody sources, which are sampled daily to calibrate the system to absolute radiance. This allows core reflectance measurements to be corrected for small core temperature differences of up to about + 5°C from ambient.

The temporal performance of the HyLogger-3 instrument and wavelength calibration of all its spectrometers are tested by comparison with a daily scan of a plate of 11 known minerals (including quartz). The TIR spectrometer in particular is calibrated with respect to wavelength by comparison with the significant quartz reflectance minimum at 8625 nm.

Table 1. Main mineral groups and minerals currently sensed by the HyLogging system, and wavelength regions for their discrimination

Mineral group	*Mineral*	*VNIR 400–1000 nm*	*SWIR 1000–2500 nm*	*TIR 6000–14 500 nm*
REE				
Iron oxide	Hematite, goethite, jarosite			
Kaolin	Kaolinite, dickite, nacrite			
White mica	Muscovite, phengite, paragonite, illite			
Smectite	Montmorillonite, nontronite, saponite			
Other AlOH	Pyrophyllite, prehnite, axinite			
	Topaz, diaspore			
	Gibbsite			
Chlorite	Fe-bearing chlorite, Mg-bearing chlorite			
Dark mica	Biotite, phlogopite			
Amphibole	Hornblende, actinolite, tremolite, riebeckite, tschermakite, edenite, grunerite, glaucophane			
Serpentine	Antigorite, chrysotile, lizardite			
Other MgOH	Mg-bearing clays, palygorskite, brucite			
	Talc			
Epidote	Epidote, clinozoisite, zoisite			
Tourmaline	Tourmaline, rubellite			
Carbonate	Calcite, dolomite, magnesite, siderite, ankerite, rhodochrosite, witherite, strontianite, smithsonite, cerussite			
Sulfate	Alunite, gypsum, anhydrite, jarosite, barite			
Phosphate	Apatite			
Borate	Vonsenite			
Oxide	Magnetite, rutile, ilmenite, cassiterite, psilomelane, pyrolusite			
Sulphide				
Quartz				
Potassic feldspar	Microcline, orthoclase, anorthoclase			
Plagioclase	Albite, andesine, oligoclase, bytownite, labradorite, anorthite			
Garnet	Grossular, andradite, uvarovite, almandine, spessartine			
Pyroxene	Augite, diopside, hedenbergite,enstatite			
Olivine	Forsterite, faylite			
Zeolite	Analcime, chabazite, heulandite, laumontite, natrolite, phillipsite			
Miscellaneous anhydrous silicates	Cordierite, andalusite, scapolite, vesuvianite			
Hydrocarbon				

LEGEND

No response
Weak or selective response
Acceptable response but other region better
Good responses but hard in mixtures
Clear unambiguous response

Table 2. HyLogger-3 TIR spectrometer characteristics

System characteristic	*Specification*
Spectrometer spectral range	6000–14 500 nm
Spectrometer spectral resolution	25–140 nm
Number of spectral channels	341 at sampling interval of 25 nm
Raw spectrometer spatial resolution	4 mm (8 mm after averaging)
Raw number of spectra per metre	250 (125 after averaging)
Typical daily acquisition rate	150–200 m
Heat sources (2)	Focused blackbody sources at a temperature of about 700°C

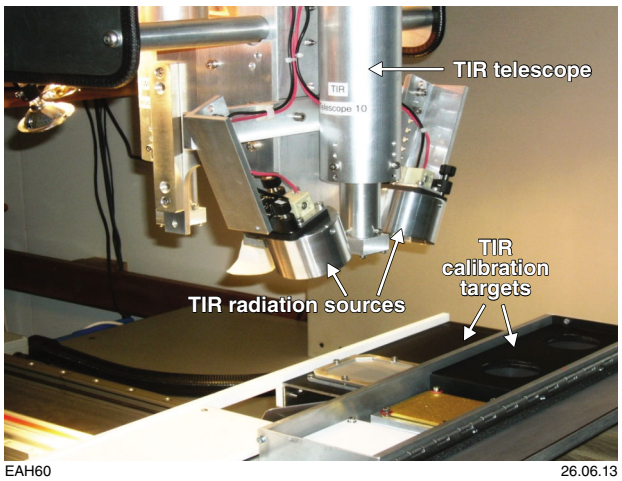

Figure 1. GSWA's HyLogger-3 TIR system: telescope, two radiation sources, and calibration unit with hot and cold blackbody sources, gold standard, Teflon, and mirror

Theoretical background

The bidirectional reflectance of a given sample ($\hat{\rho}$) is defined as follows (Schodlok et al., 2009):

$$\hat{\rho} = \rho_t \frac{V - V_b}{V_t - V_b} \qquad \text{(Equation 1)}$$

V — instrument response over the sample

V_b — instrument response when measuring the background

V_t — instrument response when measuring transfer standard

ρ_t — reflectance of the transfer standard

Temperature control

Assuming there is no source leakage into the background, the transfer standard and background are at the same temperature, and the background seen by the transfer standard and the sample are the same as the measured background, $\hat{\rho}$ is related to the sample's bidirectional reflectance, ρ, as follows:

$$\hat{\rho} = \rho + q(\Delta T) \qquad \text{(Equation 2)}$$

$q(\Delta T)$ — function of sample temperature difference

ΔT — temperature difference between the background and the sample

The bidirectional reflectance is dependent on ΔT — the hotter or colder a sample is from the background level, the greater the baseline distortion. To minimize this distortion, the temperature of any rock should therefore be at a temperature as close as possible to the background temperature prior to spectral data acquisition. For core temperature differences up to about + 5°C from ambient, the daily radiance calibration of the instrument allows quite accurate calculation of the temperature difference, and the required reflectance correction function $q(\Delta T)$. For the normal range of outside temperatures, we have established that it takes about 15 minutes for the surface of hot or cold core in a tray to reach the ambient temperature in the HyLogger room.

Light scattering

The Fresnel Equation (see Equation 3) is useful for understanding the nature of a given reflectance signature (Hapke, 2012). Significant scattering of TIR radiation from the surface of core only occurs when rays are reflected from the surface of grains without penetration. This is called 'strong surface scattering' (Fig. 2) and occurs when the extinction coefficient is much higher than the refractive index ($k >> n$). This can be seen in the standard formula for normal reflectance of a single crystal:

$$\rho = \frac{(n-1)^2 + k^2}{(n+1)^2 + k^2} \qquad \text{(Equation 3)}$$

n — real part of the complex refractive index of the material

k — imaginary part of the complex refractive index normally called the extinction coefficient

These wavelengths of high reflectance are called restrahlen features. They correspond to high values of k and their shape reflects n values less than 1, as for quartz at 8300 and 9000 nm (Wenrich and Christiansen, 1996).

In contrast, weak absorption ($k << n$) leads to low surface reflectivity and allows the radiation to enter the crystal without being immediately absorbed. In the VNIR and SWIR, where absorption is often weak, radiation is back scattered after penetrating into silicate mineral grains, as rays are refracted into grains and then reflected back out.

This is called 'volume scattering' (Fig. 2). The degree of surface scattering depends on the refractive index and absorption coefficient of the mineral, with respect to grain size and porosity of core (Salisbury et al., 1991). In wavelength regions where k is too small to force a high reflectance but high enough to absorb any radiation that enters the crystal, no radiation is scattered back to the sensor. This is called 'weak surface scattering' (Fig. 2). For example, n value for quartz at 7500 and 12 500 nm is the same as air (n=1) and incident light penetrates easily into grain resulting in low reflectance (Wenrich and Christiansen, 1996).

Data interpretation

The surface condition of drillcore strongly influences the spectral response. Wet, rough, broken, weathered surfaces and loose, fine grain sizes can complicate spectral features (Clark, 2004). For example, fine-textured particles enhance volume scattering, but reduce spectral contrast and even sometimes transform restrahlen peaks into absorption troughs (Fig. 3; Salisbury et al., 1991). Orientations of crystal cleavages or partings at the specular angle may increase reflectance values by a factor of four without significantly changing the positions of the spectral features (Schodlok et al., 2009). Large variations in spectral shape can also be caused by changes in orientation of the optical axis of birefringent minerals (Fig. 4). Minerals such as feldspar can exhibit degradation (decreasing detail and intensity) in spectral features after being subjected to natural or experimental shock, due to depolymerization of the silicate tetrahedra (Lyon, 1963; Johnson et al., 2003).

A major difficulty in interpreting TIR data arises from spectral mineral mixing, especially in the 9000–11 000 nm interval. All silicate minerals have strong reflectance spectra in this interval due to fundamental Si–O stretching vibrations. Their spectra are not always unique and can be difficult to unmix either because the spectra for two minerals are similar, or the sample spectrum is modelled equally well using more than one combination of minerals.

Of the major rock-forming minerals that are only seen in the TIR, garnet, olivine, pyroxene and quartz have unique signatures and are generally well discriminated in the data. The feldspar suite shows a range of diagnostic spectral signatures that in some cases are applicable for remote mapping or even measuring plagioclase composition (Cudahy et al., 2009). However, our experience to date with the HyLogger-3 shows that measuring feldspar information is complicated when dealing with natural mineral mixtures, especially when quartz, micas or clays are present. Only potassium feldspars and albite are generally well detected when dominant.

If only TIR data were available, it would be extremely difficult to identify many minerals that are well expressed at VNIR–SWIR wavelengths. However, the use of data from all three wavelength bands allows reasonable interpretations of the hydrous and anhydrous silicates, carbonates, sulphates and selected oxide species. It remains difficult to identify sulphides and some oxides from TIR data, but their presence may be inferred from the overall increase in TIR reflectance that these species cause.

Despite these complexities, CSIRO's mineral-library based automatic processing of TIR HyLogger-3 data can yield useful semiquantitative measurements of mineral abundances given the following assumptions:

1. Isotropic scattering occurs at all TIR wavelengths of a given drillcore sample and its mineral constituents
2. No complex fine grain size scattering phenomena
3. No uncorrected down-welling radiance or natural sample emission effects
4. Surface scattering dominates
5. Mineral mixtures can be modelled via simple linear mixing (Thomson and Salisbury, 1993).

The model used for the base reflectance data is:

$$\hat{\rho} = \sum_{m=1}^{M} f_m \rho_m + q(\Delta T) + K \quad \text{(Equation 4)}$$

f_m (m =1,2,…M) — unknown fractions of each of the M minerals in the rock

ρ_m (m =1,2,…M) — known reflectance spectra of each of the M minerals in the rock

$q(\Delta T)$ — known function of sample temperature difference

ΔT — unknown temperature difference between the background and the sample

K — unknown constant

After inversion, the fractions f_m are normalized to sum to one. In general, the constant term is small, but some minerals (especially magnetite and sulphides) can raise the overall reflectance of the sample without much change in the shape of the spectrum. In these cases examination of K profiles can be a useful method of detecting these minerals.

Software and processing

TIR, VNIR and SWIR HyLogging spectral data can be processed using the TSG-HotCore version of The Spectral Geologist (TSG) software. Previously processed datasets can be examined using the TSG Viewer software (available from <www.thespectralgeologist.com>). Mineral interpretation uses a reference set of spectra compiled with pure minerals that have been validated by XRD analyses (Schodlok et al., 2009). The current NVCL TIR reference library contains spectra for more than 70 rock-forming minerals (157 spectra; see Table 1). Other spectral reference libraries are available from Arizona State University, Johns Hopkins University, and the US Geological Survey.

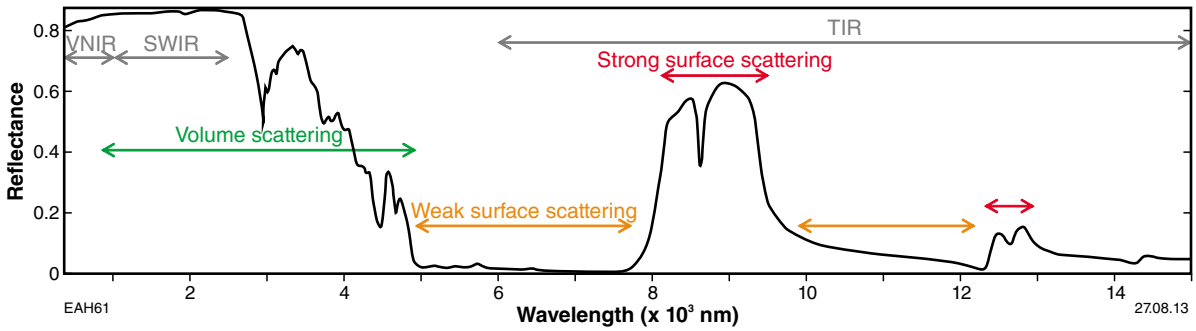

Figure 2. Scattering of light in visible-infrared region illustrated on the quartz spectrum: strong reflectance in VNIR–SWIR, volume scattering in mid-IR, and strong/weak surface scattering in TIR

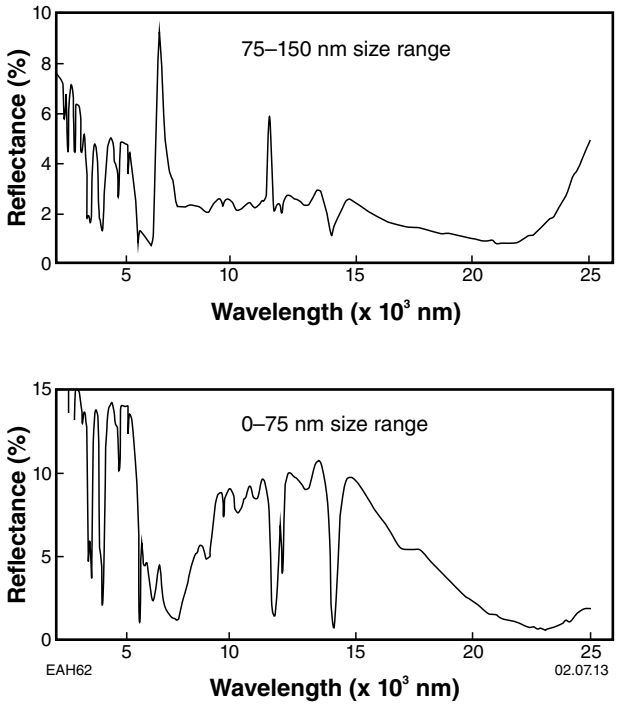

Figure 3. Infrared reflectance spectra of large and fine grains of carbonate showing volume-scattering effects. For example, peak feature transforms to a trough feature at around 11 000 nm in the fine-grained sample.

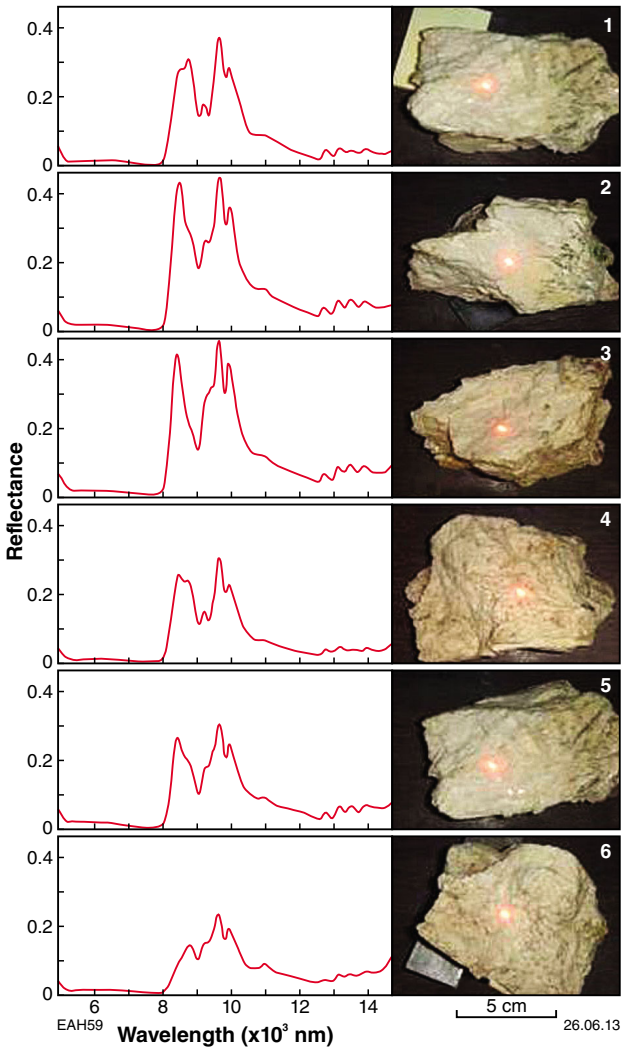

Figure 4. Spectral variations of a single albite sample (CSIRO spectral library collection)

The reference spectrum and the raw reflectance (ρ_m) for a sample are used with q to invert Equation 2, and solve for the mineral abundances (f_m) and the value of ΔT. The unknown spectrum is modelled as a mixture of three minerals per each spectral sample (about 10 mm diameter) within TSG using the TSA algorithm of Berman et al. (1999).

TIR data may also be processed by creating spectral 'scalars' or indices — parameters that target diagnostic absorption features for specific minerals or groups of minerals. This method is illustrated below for determination of quartz and carbonate abundances.

The infrared reflectance spectrum for quartz shows features arising from different radiation scattering processes (Fig. 2). The highest absorption coefficient for quartz, between 8000 and 9200 nm, is associated with the fundamental asymmetric Si–O–Si stretching vibrations. The weaker feature at 12 000–15 000 nm is attributed to symmetrical Si–O–Si stretching vibrations. The sharp characteristic 'M' absorption feature centred at 8625 nm, which is driven by the real part of the refractive index (i.e. increased volume scattering) can been used to map the relative abundance quartz in hyperspectral datasets. Two scalars were created, searching for the wavelength and the absorption depth of this feature (Fig. 5). Feldspar group minerals show additional Si–O–Al stretching vibrations, arising from replacement of some of the silicon atoms by aluminium.

The diagnostic spectral features of carbonates (Fig. 6) are caused by fundamental vibrations of the CO_3 anion. The feature between 6300 to 6800 nm is related to asymmetric stretching, and those around 11 000 to 12 000 and 13 000 to 14 000 nm are due to out-of-plane and in-plane bends, respectively (Lane and Christensen, 1997). Note that the 6300 to 6800 nm feature is in a region of strong atmospheric absorption, such that measurement using remote sensing data is not possible.

A HyLogger-3 scalar based on the height of the 6500 nm feature can be used to map carbonate occurrence even in low abundances, and to create a carbonate mask due to the lack of spectral features of other silicate minerals within that wavelength range. A scalar based on the wavelength of the 11 000 nm region feature can be applied to identify carbonate species/composition, although this can be affected by the presence of other minerals with a peak in this interval (for example, epidote), which can mask or shift the position of the CO_3 feature. A carbonate mask created on the base of the 6500 nm feature is applied to extract carbonate spectra in the 11 000 nm wavelength range. Carbonate composition can be verified using a scalar based on the 13 000 nm or longer wavelength feature, although this feature tends to be much less intense and harder to define in mixtures, especially those containing albite.

TIR spectral data can be used empirically to recognize major rock types, by applying either the Christensen Feature (CF) or the Felsic/Mafic Index (FMI) scalars in TSG. The CF can identify the general rock type for all grain-size range, and is based on the SCFM

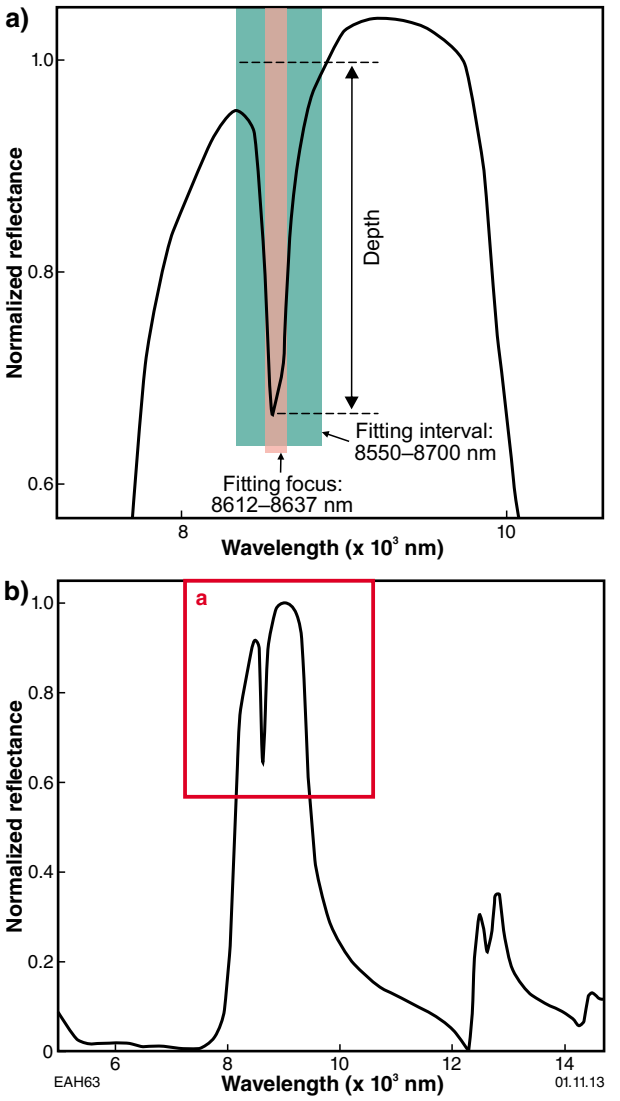

Figure 5. Quartz characteristic absorption feature at 8625 nm. It is used to map the presence of quartz and its relative abundances (depth of the feature).

chemical index of Salisbury and Walter (1989): $SCFM = SiO^2/(SiO^2+CaO+FeO+MgO)$. The CF occurs in a wavelength region of minimum reflectance and absorption where the refractive index of silicates approaches 1 due to anomalous dispersion, at wavelengths just shorter than those of the Si–O bond stretching vibration (Fig. 7a). Spectral features related to Si–O bond strength are systematically shifted with changes in degree of polymerization of the SiO_4 ion. This results in fundamental vibrations at shorter wavelengths for framework silicates, and at longer wavelengths for tetrahedra (Fig. 7b).

A related FMI scalar extracts the wavelength of the 'overall' reflectance maximum of the whole rock spectrum (Fig. 8a). It is used here to interpret bulk rock composition using the same principle as for the CF — increasing silica content from mafic to felsic rocks is reflected by a shift of spectral features towards shorter wavelengths (Fig. 7b).

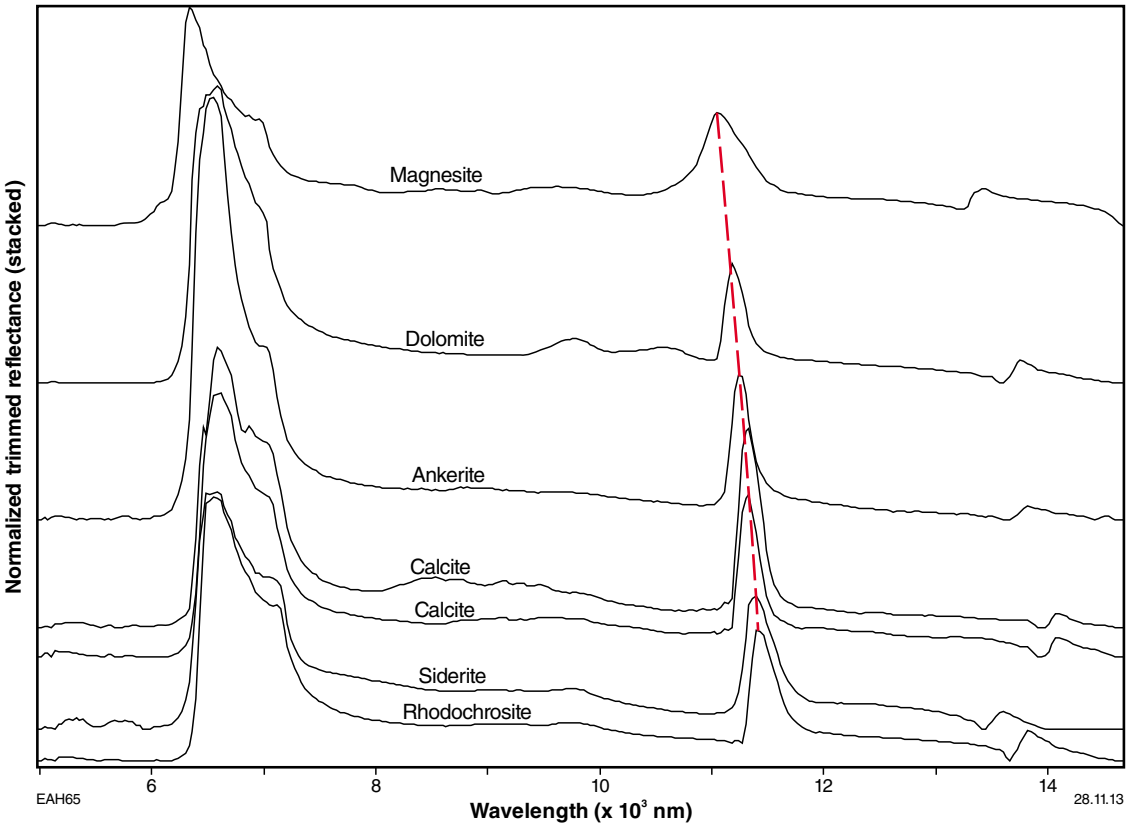

Figure 6. Spectra of major anhydrous carbonates. From top to bottom: magnesite, dolomite, ankerite, calcite, siderite, rhodochrosite.

Note that carbonate spectra can strongly affect the TSG FMI scalar, and are normally automatically masked out in this algorithm. As noted earlier carbonates can be successfully mapped with their own scalars.

To illustrate the power of the FMI bulk rock-type characterization, Figure 8b shows a greater degree of variation. This dataset from the Windimurra complex (Murchison Terrane, Yilgarn Craton) illustrates narrow quartz-bearing intervals with short wavelength FMI values, medium wavelength chlorite + plagioclase and long wavelength olivine bearing intervals. The scalar also emphasizes many cyclical intervals in the lower part of the hole providing guidance for more detailed analysis.

Even though the CF and FMI approaches were originally developed for igneous rocks, they have proved to be valuable for characterizing and 'domaining' (identifying blocks of similar coherent spectra) drillcores containing a range of felsic, mafic, ultramafic and skarn minerals. It has also been our experience that the FMI is more robust and less prone to noise and volume scattering effects than the CF. TSG offers scalars for both methods and they can easily be compared.

Data volume

Addition of the TIR spectrometer to the HyLogger instrument has increased the volume of processed data by about 20%, from about 330 MB per 100 m of drillhole scanned, to about 400 MB per 100 m. The volume of raw data, including TSG Quality Control (QC) files, increases by 10% to about 1400 MB per 100 m. Thus, hyperspectral data and high-resolution images for each 100 m of scanned and processed core will occupy about 1.8 GB of storage space.

Applications for exploration

Geological surveys, the academic research sector, and exploration/mining companies currently use HyLogging data in combination with high-resolution images for objective mineralogical logging of drillcore. The new TIR spectrometer in HyLogger-3 instruments extends this capacity, and we showcase here the application of this new TIR mineral information for two mineral prospects in Western Australia:

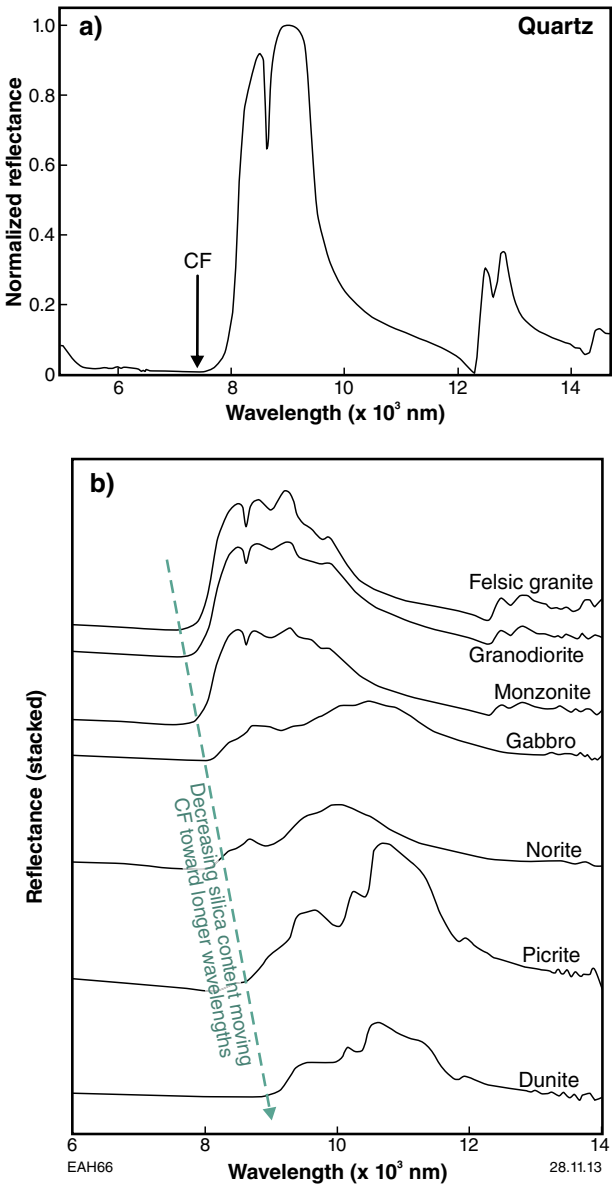

Figure 7. Christensen Feature (CF) for mapping igneous rock types: a) location CF on quartz spectrum; b) moving CF toward longer wavelengths with decreasing silica content

- Minnie Springs Mo–Cu–W — an analysis of alteration assemblages and vectors to mineralization
- Cummins Range REE — identification of important rock-forming and ore-hosting minerals.

Minnie Springs Mo–Cu–W prospect

The geology of the Minnie Springs prospect, and the results of a HyLogger SWIR study of core from the deposit, have been previously described and discussed by Hancock and Huntington (2010), and are only briefly summarized here.

Minnie Springs is located in the northwest-trending Ti Tree Shear Zone of the Paleoproterozoic Gascoyne Province of Western Australia (Fig. 9). The zone of disseminated and quartz vein-hosted Mo–Cu–W mineralization is over 1 km long, more than 100 m wide and at least 150 m deep. Mineralization is largely hosted by biotite monzogranite affected by silica and alkali metasomatism and related quartz-sericite-chlorite alteration (Pirajno et al., 2008).

Nine holes have been drilled along the zone of Mo mineralization (>25 ppm). The central holes (MSD1, MSD2, MSD3, MSD4, and MSD5) are located along the boundary of a cupola-like granite at its intersection with a north-trending fault that hosts mafic dykes and quartz veins. Three stages of alteration are recognized in the granitic rocks (Pirajno and Hancock, unpublished data) as follows:

1. Dominant potassic alteration, comprising microcline and biotite, and associated with disseminated molybdenite mineralization with an age of 1770 Ma (Pirajno et al., 2008). This stage represents potassic metasomatism that occurred in the apical portions of granitic cupola-like intrusions that emanated from the Minnie Creek batholith

2. Sericitic (phyllic) alteration, characterized by silica-muscovite-pyrite veins caused by hydrothermal fluids that evolved from the greisen system during Ti Tree Shear Zone deformation

3. Propylitic alteration, comprising low temperature quartz, chlorite, epidote, and carbonate assemblages that formed from transitional hydrothermal fluids, and that locally retrogressed the sericitic alteration. Quartz veins with massive molybdenite mineralization and rare carbonate veinlets formed during this later alteration stage.

HyLogging data have contributed to building the alteration model for the Minnie Springs prospect. VNIR–SWIR spectrometry clearly identified:

- the dominant white mica and chlorite characteristics of phyllic and propylitic alteration
- near-surface oxidization down to a depth of 10–25 m, based on the presence of well- and poorly ordered kaolinite
- the change in Fe-oxide composition from hematitic at the surface to goethitic at depth.

Recent rescanning of all nine drillholes (1500 m of core) using the TIR spectrometer, provided new information on the distribution of feldspar minerals, quartz, and carbonate. The following description is a part of 3D modelling of the HyLogging mineralogy for the Minnie Springs prospect in cooperation with Dr Maarten Haest from WA Centre of Excellence for 3D Mineral Mapping (C3DMM), CSIRO.

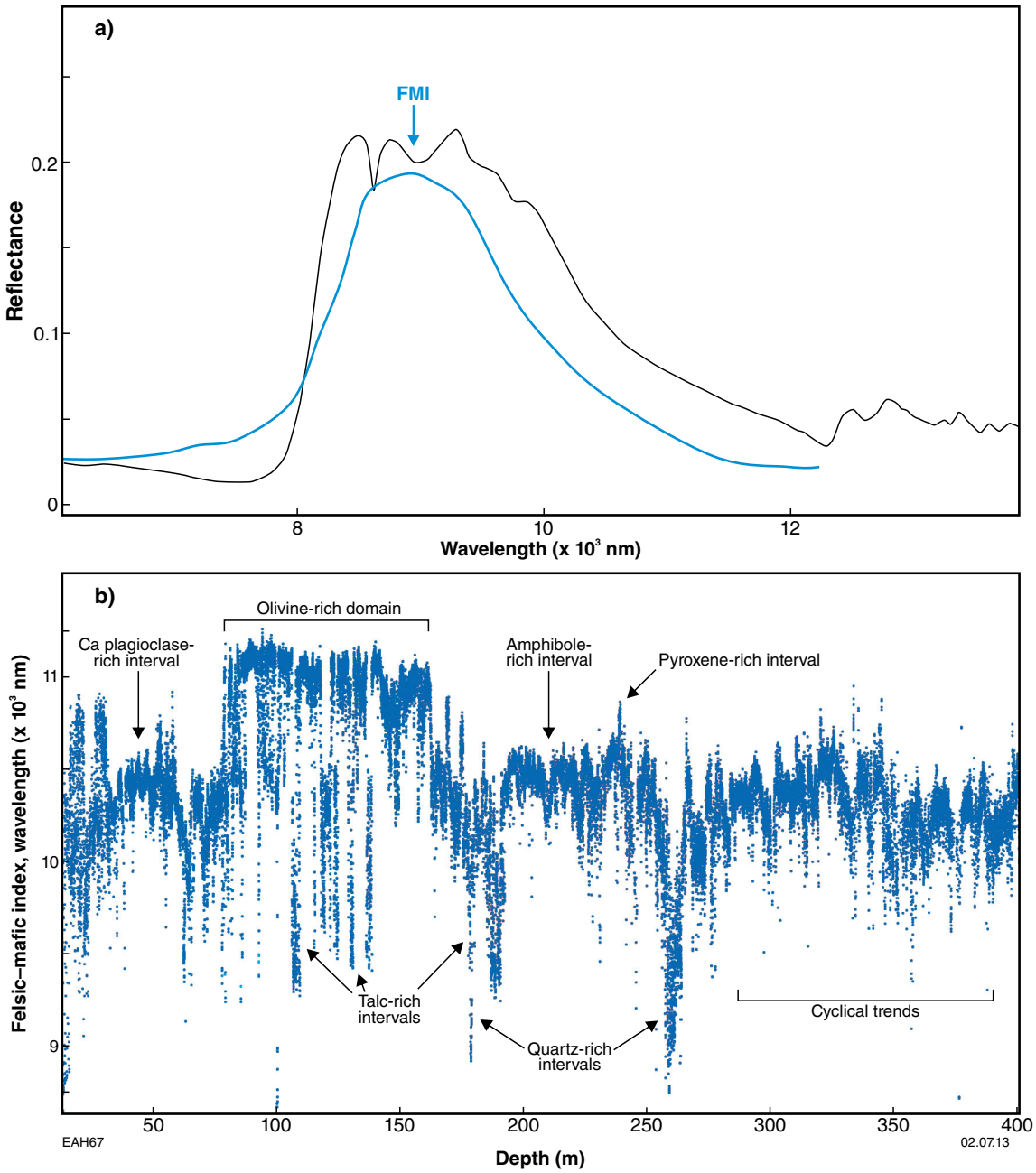

Figure 8. **Felsic–mafic Index (FMI): a) overall reflectance maximum of the whole-rock spectrum as the summary of the individual rock-forming minerals; b) FMI for Windimurra drillhole MNDD0002. The major compositional domains and trends from the more felsic (low in the plot) with short wavelength reflectance peaks, through intermediate, mafic and ultramafic mineral associations (at the top of the plot). Mineral labels based on obvious matches to library spectra. Carbonate-bearing samples are not shown.**

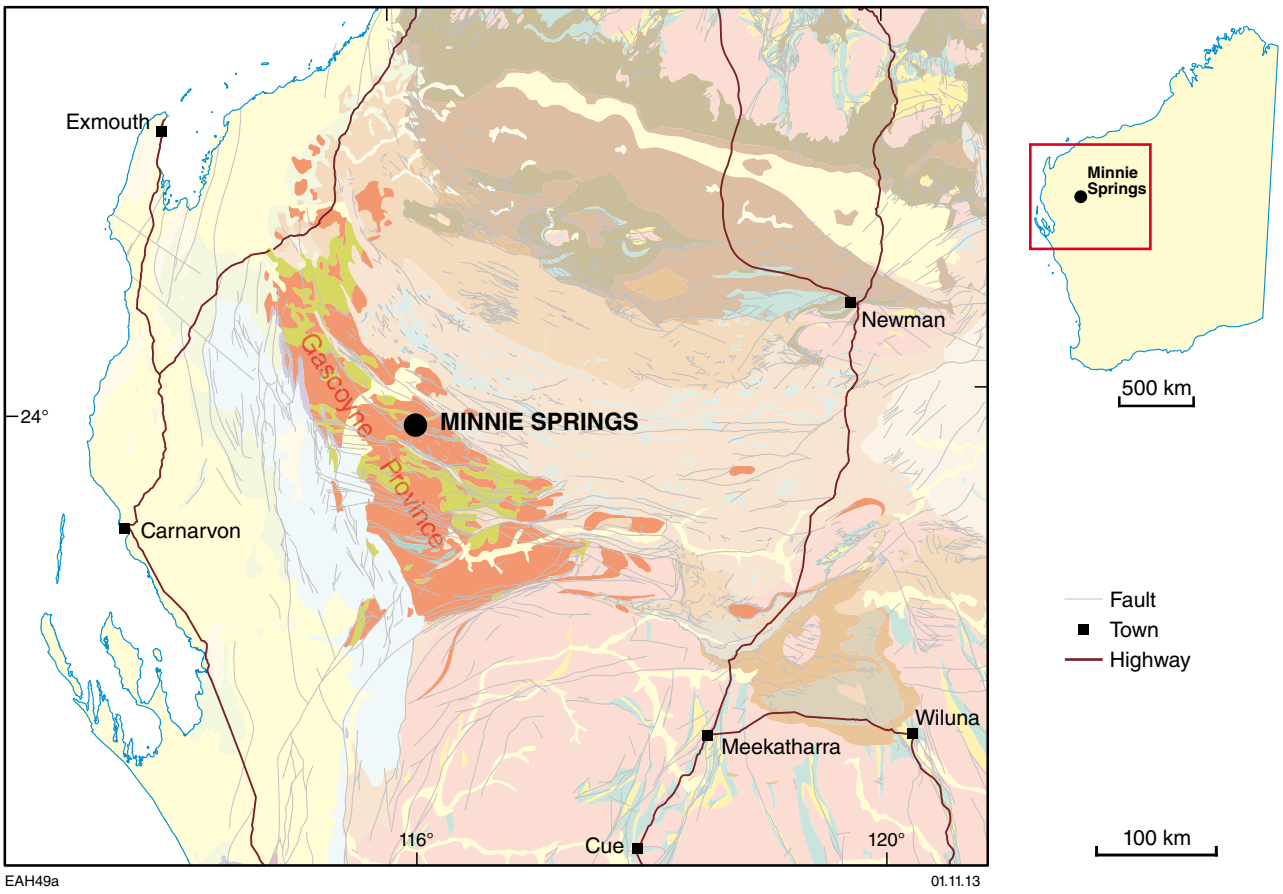

Figure 9. Geological location of the Minnie Springs molybdenum–copper prospect

Minerals detected with the TIR system

Feldspar

According to petrographic study, albite has been extensively altered by the later stage of sericitic alteration. However, it has been detected at 130–190 m depth within granodiorite in the central part of the prospect (Fig. 10). This zone is spatially correlated with elevated levels of molybdenum mineralization. Albite is also recognized in granites along the shear zone, persisting to the surface in the southeast and limited towards the northwest. Microcline is a significant component of core in all drillholes except the central albite zone. In the northwest outcrop, the granite shows strong microcline alteration with a pink appearance.

The image depicting the relative distribution of microcline and albite is built using Leapfrog software, using the EUDAMULLAH 1:100 000 Geological Series map sheet as the base to the 3D image (Fig. 11). There is strong correlation between the relative distribution of feldspar at the surface and mapping of K-feldspar and plagioclase-rich granites.

Quartz

Quartz is a main constituent of the host rocks, and also pervades in sets of veins within the Ti Tree Shear Zone that hosts massive Mo mineralization. A distinction between vein-hosted and granitoid-hosted quartz is made on the basis of a 1900 nm feature that is attributed to water absorption in fluid inclusions in the hydrothermal quartz (Fig. 12). There is positive correlation between mineralization and quartz vein distribution, although some veins do not have significant Mo concentration. The rest of molybdenum mineralization is disseminated in monzogranite.

Carbonate

The TIR spectra show only sparse calcite veining and limited correlation of this with mineralization. Previous XRD analyses confirmed the lack of carbonates in Minnie Springs core.

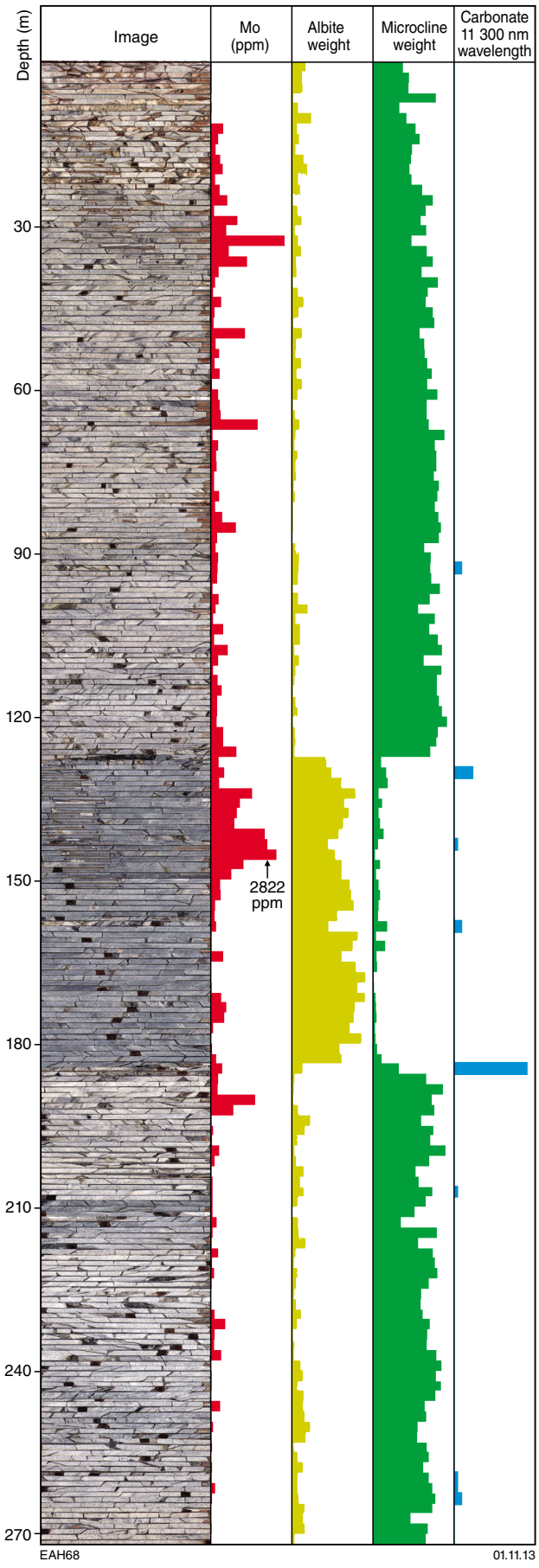

Figure 10. **(left) TSG logs for Minnie Springs core, drillhole MSD2: core trays image, molybdenum assay, and relative abundances (per 2 m interval) of albite, microcline, and carbonate**

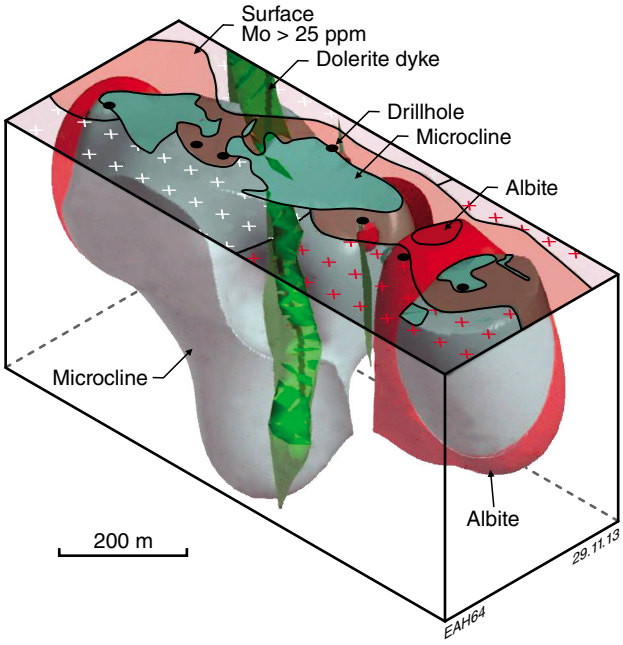

Figure 11. **3D relative distribution of microcline (pale green) and albite (red) with the geological map of Minnie Springs prospect. Microcline is prominent at the surface in the area mapped as K-feldspar-rich granite (white crosses) and albite zone distributes at the surface in the area mapped as plagioclase-rich granite (red crosses). Courtesy of Maarten Haest, C3DMM, CSIRO (unpublished image).**

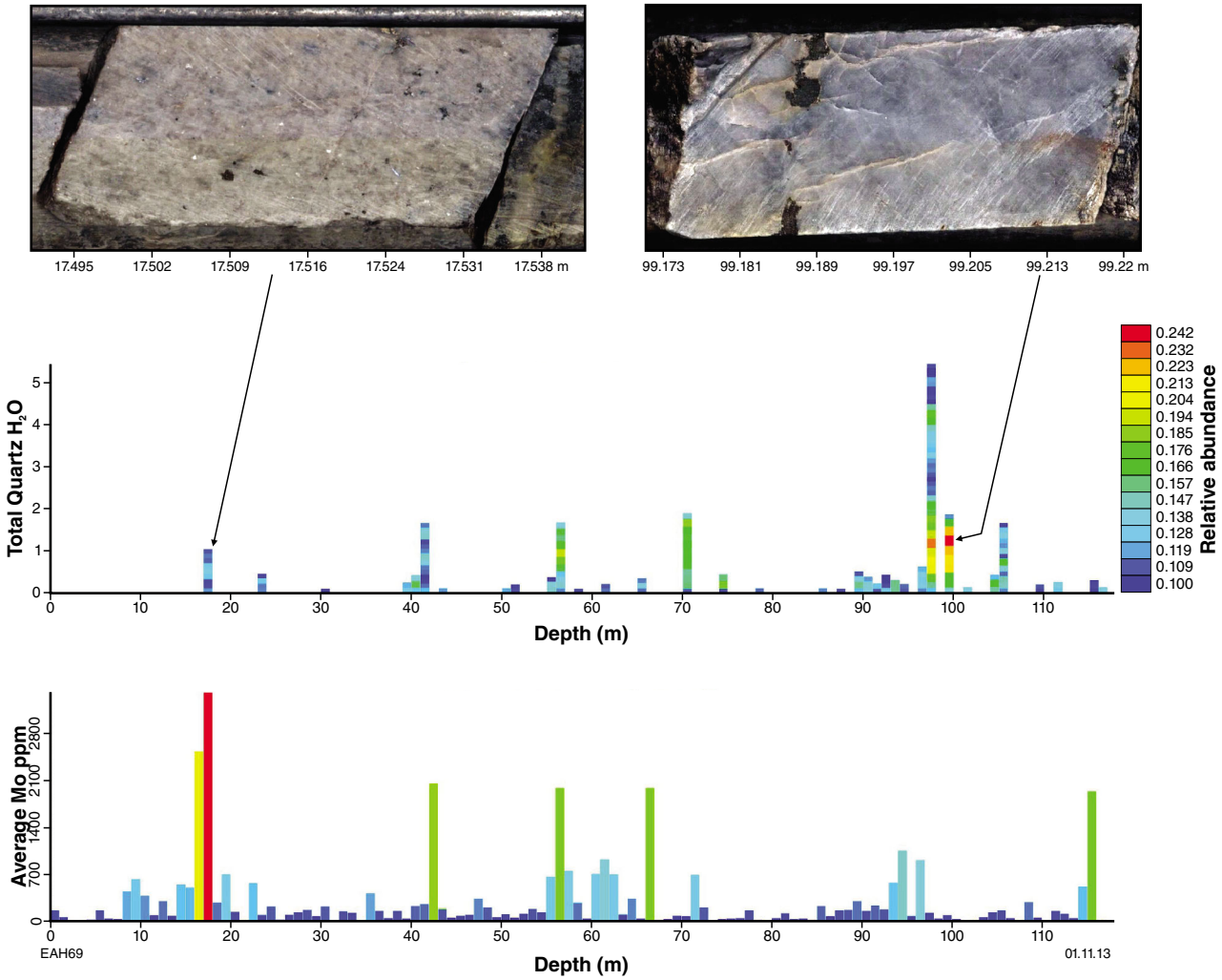

Figure 12. The top histogram shows distribution of quartz veins extracted from 1900 nm scalar. High water content (red) and lower water content (blue) refer to depth of 1900 nm quartz feature that is associated with abundance of fluid inclusions in quartz. In comparison, the bottom histogram shows assay results for Mo mineralization along the hole. Core images represent the highest mineralized interval with disseminated molybdenite (left) and highest water content in vein quartz with lack of Mo mineralization (right). Minnie Springs, drillhole MSD1.

Cummins Range REE prospect

The Cummins Range Carbonatite is located in the southern Halls Creek Orogen adjacent to the Kimberley Craton, Western Australia (Fig. 13). It is a Neoproterozoic diatreme consisting of three concentric zones: unaltered pyroxenite, mica-rich pyroxenite, and a central plug of carbonatite (Sanders, 1999). The main REE-bearing minerals are residual primary monazite and apatite concentrated in the oxidized zone; secondary REE enrichment has played a subordinate role (Sweetapple and Downes, 2010).

HyLogging data for two holes drilled in the carbonatite central plug show variable proportions of Ca-amphiboles, phlogopite, and Mg-chlorite in carbonate matrix (Fig. 14). Lithologically these intervals refer to the altered pyroxenites and amplified by darker images. Clinopyroxenes appear sporadically below 336 m, and their amount gradually increases with depth. TIR spectra have been used to calculate abundance and composition of carbonates (Fig. 15), and show the presence of dolomite (blue tones) and subordinate amounts of calcite and siderite (green and yellow).

Detailed mineralogical logging

HyLogging data contribute to mapping minerals in the core that are difficult to distinguish with the naked eye. Assay results from the prospect indicate that the major REE mineralization occurs in the oxidized zone down to 90 m deep, where jasperoidal ironstone breccias contain a significant amount of fluorapatite and monazite-(Ce) (Sweetapple and Downes, 2010). We used 740 nm and 800 nm wavelengths diagnostic absorption features for

light rare earth minerals (LREE) (Morin-Ka, 2012) to create scalars for searching abundance of these minerals. The resulting histograms show high concentrations of REE in the oxidized zone, although primary carbonates also have elevated amounts of REE-bearing minerals (Fig. 16, columns 3 and 4). This distribution pattern correlates well with the cerium assays (Fig. 16, column 2). The absorption features at 740 nm and 800 nm relate to crystal-field transitions of electrons in REE ions, and do not change for different host minerals (Clark, 2004). It is therefore difficult to discriminate between apatite, bastnaesite, parasite, and other LREE-bearing minerals using these features (Morin-Ka, 2012).

Another option in identifying specific minerals using TSG is to match the spectra to those for specific minerals in spectral reference libraries (Auxiliary Match). This method can be used only as a guide to the presence of particular minerals in the Cummins Range core because of their small grain size and mixing of spectra. We nevertheless applied the technique to search for apatite, monazite, and bastnaesite, and also for other minerals observed in the core — zircon, richterite, and ilmenite (but not magnetite, which though known to be present in the pyroxenites, has low spectral response in the HyLogger range, especially in mixtures, and is better detected using its magnetic properties).

The best results were obtained for apatite (Fig. 16, column 5). Apatite has a large grain size and diagnostic spectral features in the TIR range; hence, it is more easily detected with high probability by matching to existing spectra in the TIR reference library. TIR spectra for zircon and richterite are less useful, due to mixing problems at wavelengths around 9000 to 10 000 nm. Nevertheless zircon was detected using its diagnostic features at VNIR and richterite was extracted on the basis of its amphibole features at SWIR. The ilmenite TIR spectrum was discovered in the Cummins Range dataset. The sample was validated by SEM-EDX and its TIR spectrum was

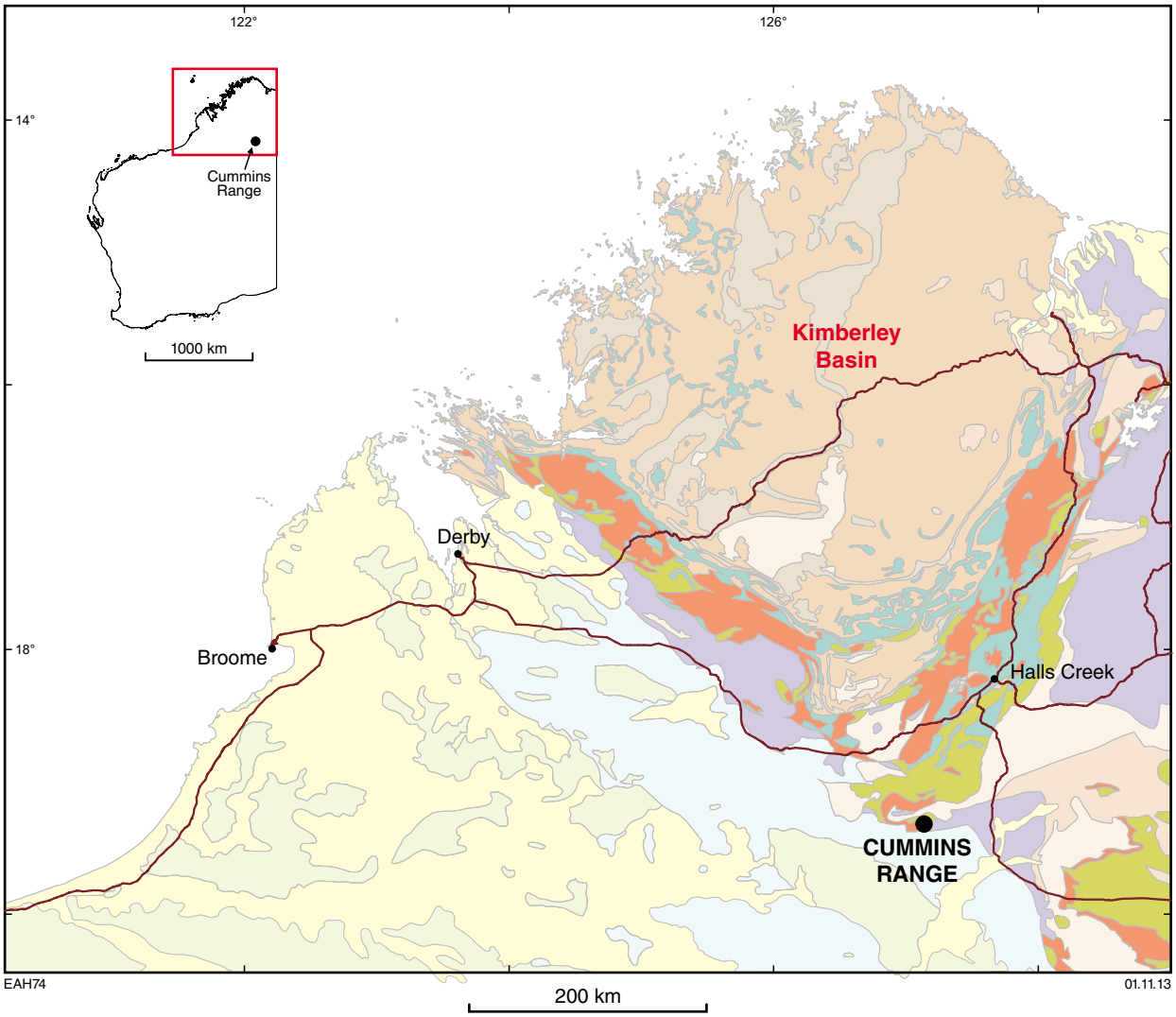

Figure 13. Geological location of the Cummins Range REE prospect (data from GeoVIEW.WA)

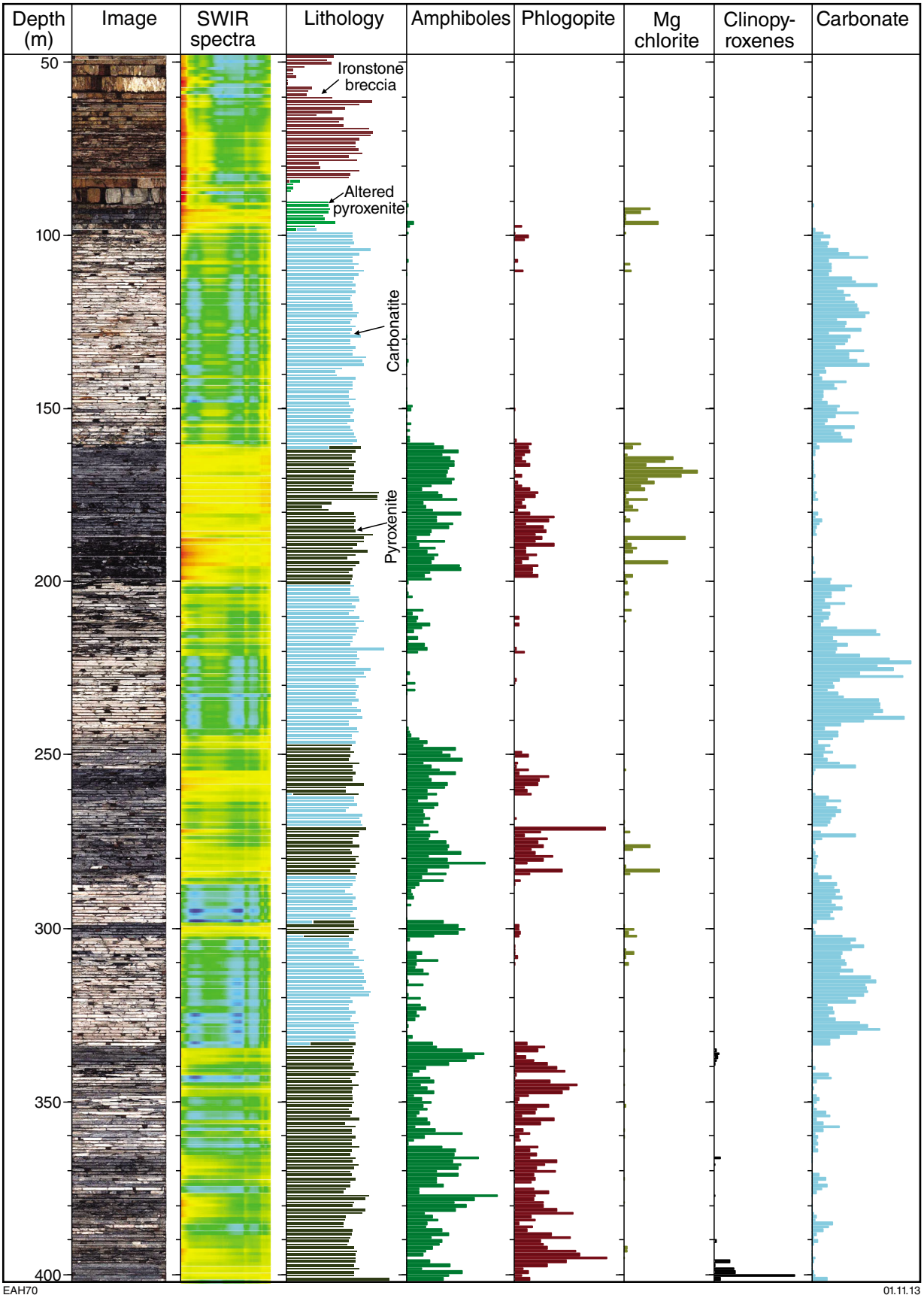

Figure 14. TSG logs for Cummins Range core, drillhole DD84CDD1: core trays image, SWIR spectra, company lithology logging, and relative abundances (per 1 m interval) of amphibole, phlogopite, Mg-chlorite, clinopyroxene, and carbonate

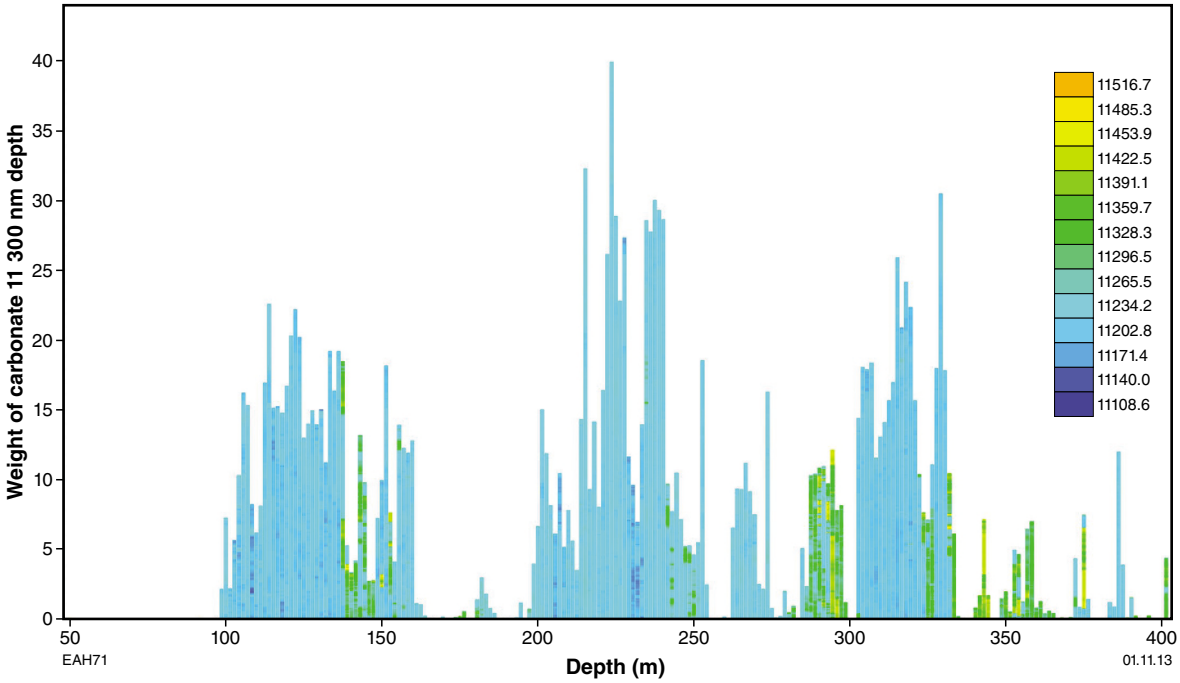

Figure 15. TSG log for Cummins Range core, drillhole DD84CDD1: relative abundance (per 1 m interval) and composition of carbonates calculated on depth and wavelength of spectral feature at 11 300 nm. Shorter wavelengths (blue colour) refer to dolomite, longer wavelengths (green and yellow) — to calcite and ankerite. Colour bar indicates change in wavelength of selected spectral feature with representative values given within each grade.

added to the TSG spectral reference library. The relative abundance of ilmenite interpreted from the Cummins Range dataset is shown on Figure 17a.

The distribution of pyrrhotite was successfully mapped using the TIR HyLogging scalar 'Background Offset' (TirBkgOffset) (Fig. 17b), and that for other sulphides was estimated from the increase in overall reflectance as calculated in Equation 4.

Conclusion

The addition to the new generation HyLogger-3 instrument of a TIR spectral reflectance sensing system suited to anhydrous silicates has achieved the following:

- increased the ability to rapidly, objectively, and non-destructively log rock-forming and alteration minerals in drillcore
- differentiate igneous rock types
- improve VNIR–SWIR data interpretations.

Processing and interpreting TIR data is more complex compared with the VNIR and SWIR data. However, the process is being streamlined with new TSG analysis techniques and more expansive mineral reference libraries; the processing and interpreting burden is more than offset by having unique, 10 mm, co-registered mineral spectral data that is far more representative of the complete range of geological compositions than was previously possible.

The principal benefits of the new TIR system include the ability to sense minerals such as quartz and feldspar (in addition to pyroxene, olivine, and garnet) that were previously undetectable in VNIR–SWIR data, and to more accurately identify carbonates than was possible using SWIR data alone. Other specific geological applications of the GSWA HyLogger-3 developed so far include mapping of apatite and other REE-bearing minerals in carbonatites, and detecting variations in feldspar species in altered rocks. It is also possible to demonstrate differentiation of pyroxene- and olivine-bearing mafic–ultramafic sequences, and to identify garnets in selected high-grade gold deposit environments in the Yilgarn (Huntington et al., 2008).

Acknowledgements

The GSWA HyLogging system was funded by CSIRO, as part of the federally funded NVCL, administered by AuScope Pty Ltd. The NVCL is one component of the AuScope Earth Model. The innovation and assistance of the CSIRO HyLogging Technologies development team is sincerely appreciated. We gratefully acknowledge all parties to this CSIRO–GSWA–AuScope collaboration. We also thank Thomas Cudahy (CSIRO) for improving the Record with his insightful comments and additions.

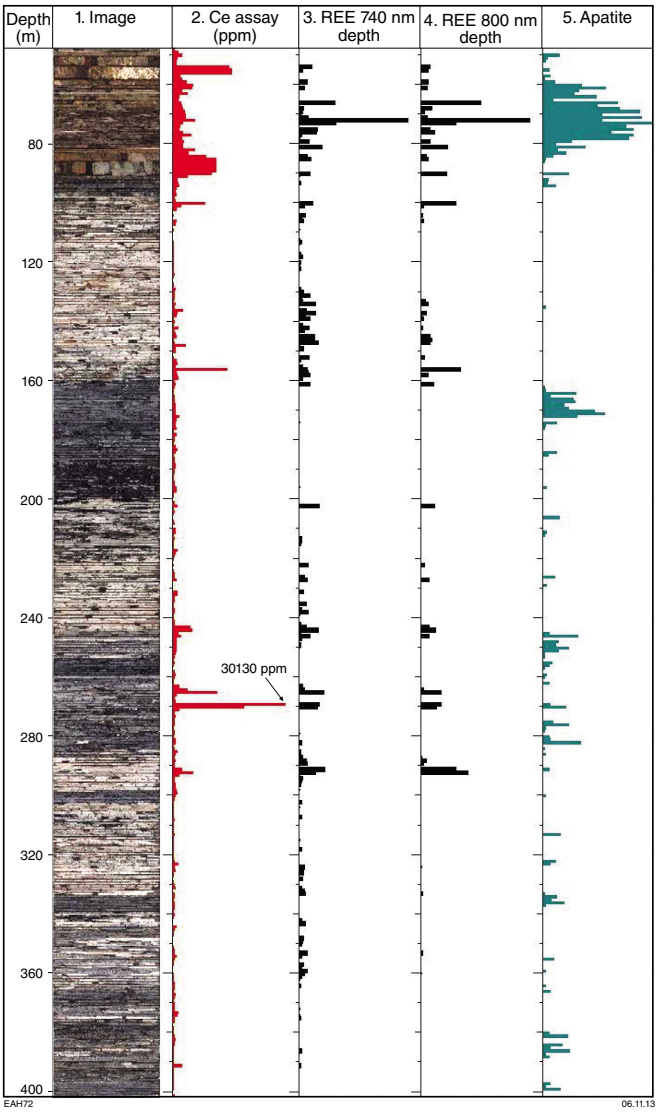

Figure 16. TSG log for Cummins Range core, drillhole DD84CDD1: core tray image, Ce assay, and relative abundances (per 1 m interval) of REE (calculated on depth of absorption features at 740 nm and 800 nm) and apatite

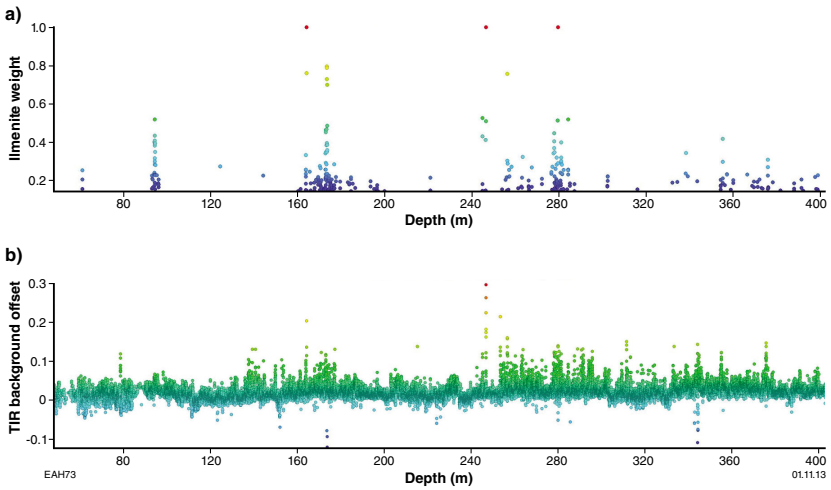

Figure 17. TSG log for Cummins Range core, drillhole DD84CDD1: a) relative abundance (per 2 m interval) of ilmenite; b) distribution of pyrrhotite showing by yellow-red dots rising above the blue background level

References

Berman, M, Bischof, L and Huntington, JF 1999, Algorithms and software for the automated identification of minerals using field spectra or hyperspectral imagery: Proceedings of the 13th International Conference on Applied Remote Sensing, Vancouver, Canada, 1 March 1999, p. 222–232.

Clark, RN 2004, Spectroscopy of rocks and minerals, and principles of spectroscopy, *in* Manual of remote sensing, Volume 3: remote sensing for the earth sciences (3rd edition) *edited by* AN Rencz and RA Ryerson: John Wiley and Sons, Inc., New York, USA, p. 3–58.

Cudahy, TJ, Hewson, RD, Caccetta, M, Roache, A, Whitbourn, LB, Connor, P, Coward, D, Mason, P, Yang, K, Huntington, JF and Quigley, MA 2009, Drill core logging of plagioclase feldspar composition and other minerals associated with Archaean gold mineralisation at Kambalda, Western Australia using a bidirectional thermal infrared reflectance system: Economic Geology, v. 16, p. 223–235.

Hancock, EA and Huntington, JF 2010, The GSWA NVCL HyLogger: rapid mineralogical analysis for characterizing mineral and petroleum core: Geological Survey of Western Australia, Record 2010/17, 21p.

Hapke, B 2012, Theory of reflectance and emittance spectroscopy: Cambridge University Press, New York, USA, 528p.

Huntington, JF, Whitbourn, LB, Quigley, MA, Yang, K, Mason, P, Cudahy, TJ, Connor, P, Coward, D, Hewson, R and Phillips, R 2008, Development and implementation of advanced automated core logging technology for enhanced mine feasibility and development in Western Australia: MERIWA Project M373, Report 269, 41p.

Johnson, JR, Hoerz, F and Staid, MI 2003, Thermal infrared spectroscopy and modelling of experimentally shocked plagioclase feldspars: American Mineralogist, v. 88, p. 1575–1583.

Lane, MD and Christensen, PR 1997, Thermal infrared emission spectroscopy of anhydrous carbonates: Journal of Geophysical Research, v. 102, p. 25581–25593.

Lyon, RJP and Burns, EA 1963, Analysis of rocks and minerals by reflected infrared radiation: Economic Geology, v. 58, p. 274–284.

Morin-Ka, S 2012, Hyperspectral characterization of rare earth minerals: Geological Survey of Western Australia, Record 2012/12, 50p.

Pirajno, F, Sheppard, S, Groenewald, PB and Johnson, SP 2008, Mineral systems in the Gascoyne Complex, Western Australia, *in* GSWA 2008 extended abstracts: promoting the prospectivity of Western Australia: Geological Survey of Western Australia, Record 2008/2, p. 4–7.

Salisbury, JW and Walter, LS 1989, Thermal Infrared (2.5 – 13.5 μm) spectroscopic remote sensing of igneous rock types on particulate planetary surfaces: Journal of Geophysical Research, v. 94, p. 9192–9202.

Salisbury, JW, Walter, LS, Vergo, N and D'Aria, DM 1991, Infrared (2.1-25 μm) spectra of minerals: The Johns Hopkins University Press, Baltimore and London, 266p.

Sanders, TS 1999, Mineralization of the Halls Creek Orogen, east Kimberley region, Western Australia: Geological Survey of Western Australia, Report 66, 44p.

Schodlok, MC, Green AA, Huntington, JF and Whitbourn, LB 2009, A new library of thermal infrared reflectance spectra of rock-forming minerals and rocks, *in* 6th Workshop on Imaging Spectroscopy: An Innovative Tool for Scientific and Commercial Applications: Tel Aviv, Israel, p. 6.

Sweetapple, M and Downes, PJ 2010, Petrographic and mineralogical studies of ten samples from the oxidised zone of the Cummins Range carbonatite, Western Australia: CSIRO, Report P20/525, 56p.

Thomson, JL and Salisbury, JW 1993, The mid-infrared reflectance of mineral mixtures (7–14 um): Remote Sensing of Environment, v. 45, p. 1–13.

Wenrich, ML and Christensen, PR 1996, Optical constants of minerals derived from emission spectroscopy: Application to quartz: Journal of Geophysical Research, v. 101, p. 15921–15931.

Appendix 1

Mineral and petroleum core processed through the GSWA HyLogger showing only core stored in the GSWA Core Libraries

Hole name	*Project*	*Commodity*	*Location*	*Total (m)*	*EIS*	*TIR*
AB62	Abra	Pb–Ag	Edmund Basin	600.9	✓	✓
HY2	Abra, Greater Hyperion	Pb–Ag	Edmund Basin	638.5	✓	✓
Acacia 1	Acacia	Petroleum	Canning Basin, Barbwire Terrace	1169.7		
Acacia 2	Acacia	Petroleum	Canning Basin, Barbwire Terrace	66.4		✓
CRA DD87SS7	Admiral Bay	Pb–Zn	Canning Basin, Willara Sub-basin	581.3		
ABDP1	Archean Biosphere Drilling (Japanese)		Pilbara Craton, Marble Bar	264		
ABDP2	Archean Biosphere Drilling (Japanese)		Pilbara Craton	249		
ABDP3	Archean Biosphere Drilling (Japanese)		Fortescue Basin	150		
ABDP4	Archean Biosphere Drilling (Japanese)		Fortescue Basin	195		
ABDP5	Archean Biosphere Drilling (Japanese)		Pilbara Craton	195		
ABDP5B	Archean Biosphere Drilling (Japanese)		Pilbara Craton	14.6		
ABDP6	Archean Biosphere Drilling (Japanese)		Fortescue Basin	287.2		
ATD101	Austin Deeps	Cu–Zn–Au–Ag	Murchison Terrane	556	✓	
Barbwire 1	Barbwire	Petroleum	Canning Basin, Barbwire Terrace	8.3		✓
Blina 4	Blina	Petroleum	Canning Basin, Lennard Shelf	15.5		
Blina 3	Blina	Petroleum	Canning Basin, Lennard Shelf	54		
Blina 5	Blina	Petroleum	Canning Basin, Lennard Shelf	12		
Boab 1	Boab	Petroleum	Canning Basin, Barbwire Terrace	1022.2		
BRWD0019	Browns Range	REE	Kimberley	220.9		✓
Canopus 1	Canopus	Petroleum	Canning Basin, Mowla Terrace	8.4		✓
Cassia 1	Cassia	Petroleum	Canning Basin, Barbwire Terrace	1445.1		
Cleaverville 1	Cleaverville – Dixon Island		West Pilbara Superterrane	65.9		
Cleaverville 2	Cleaverville – Dixon Island		West Pilbara Superterrane	44.4		
Cleaverville 3 DX	Cleaverville – Dixon Island		West Pilbara Superterrane	100.6		
Cliff Head 6	Cliff Head	Petroleum	Perth Basin, Abrolhos Sub-basin	34		
Harvey1	Collie CO_2 hub	Petroleum	Perth Basin	216.4		✓
Cody 1	Cody	Petroleum	Carnarvon Basin, Exmouth Gulf	37.1		
DD84CDD1	Cummins Range	REE	Halls Creek Orogen	354.1		✓
DD84CDD2	Cummins Range	REE	Halls Creek Orogen	357		✓
CDD001	Cundeelee	REE	Yilgarn Craton	5.9		✓

Appendix 1. continued

Hole name	*Project*	*Commodity*	*Location*	*Total (m)*	*EIS*	*TIR*
JD01	Cundeelee	REE	Yilgarn Craton	5.9		✓
DS09RMD001	Darkstar	Au	Yilgarn Craton	673.3	✓	✓
DS09RMD002	Darkstar	Au	Yilgarn Craton	440.4	✓	✓
ABDP10	Deep Time Drilling (Japanese)		Pilbara Craton	207.3		
ABDP8	Deep Time Drilling (Japanese)		Pilbara Craton	311.5		
ABDP9	Deep Time Drilling (Japanese)		Hamersley Basin	880.1		
Eremophila1	Eremophila1	Petroleum	Canning Basin, Barbwire Terrace	1135.3		✓
HDDH001	Eucla, Haig prospect	Fe–Cu–Au	Eucla Basin	323.8	✓	✓
HDDH002	Eucla, Haig prospect	Fe–Cu–Au	Eucla Basin	214.4	✓	✓
NDDH002	Eucla, NSD prospect	Fe–Cu–Au	Eucla Basin	225.5	✓	✓
Ficus 1	Ficus	Petroleum	Canning Basin, Barbwire Terrace	1045.5		
FMM397	Fraser, Southern Cross	Au	Yilgarn Craton	106.8		✓
Cockburn 1	Geothermal		Perth Basin, Mandurah Terrace	80		
GinGin1	GinGin1	Petroleum	Perth Basin	81.5		✓
CUDD001	Golden Grove	Pb–Zn	Murchison Terrane	935.7		✓
GG274	Golden Grove	Pb–Zn	Murchison Terrane	555.5		✓
GG276D1	Golden Grove	Pb–Zn	Murchison Terrane	290		✓
RHDD034	Golden Grove	Pb–Zn	Murchison Terrane	412.9		✓
SC098D1	Golden Grove	Pb–Zn	Murchison Terrane	648.5		✓
SC107	Golden Grove	Pb–Zn	Murchison Terrane	544.4		✓
GPD1464	Golden Pig, Southern Cross	Au	Yilgarn Craton	109.3		✓
Donnybrook DNB1	Government Quarry		Perth Basin, Bunbury Trough	29.78		
Donnybrook DNB2	Government Quarry		Perth Basin, Bunbury Trough	14.74		
Donnybrook DNB3	Government Quarry		Perth Basin, Bunbury Trough	15.22		
Donnybrook DNB4	Government Quarry		Perth Basin, Bunbury Trough	12.15		
GSWAWOODLEIGH 1	GSWA stratigraphic		Southern Carnarvon Basin	142.6		✓
NLD 046	Hercules	Au	Albany–Fraser Orogen	170.4	✓	✓
NLD 069	Hercules	Au	Albany–Fraser Orogen	70.5	✓	✓
NLD 070	Hercules	Au	Albany–Fraser Orogen	87	✓	✓
NLD 071	Hercules	Au	Albany–Fraser Orogen	71.8	✓	✓
NLD 080	Hercules	Au	Albany–Fraser Orogen	47.9	✓	✓
NLD 097	Hercules	Au	Albany–Fraser Orogen	85.9		✓
NLD 210	Hercules	Au	Albany–Fraser Orogen	170		✓
Hovea 3	Hovea 3	Petroleum	Perth Basin, Dandaragan Trough	81.26		✓

Appendix 1. continued

Hole name	*Project*	*Commodity*	*Location*	*Total (m)*	*EIS*	*TIR*
JDH01	Jubuk	Fe	South West Terrane, Yilgarn Craton	112.6	✓	
Kunzea 1	Kunzea	Petroleum	Canning Basin, Broome Platform	441.5		
LFDD001	Lake Lefroy	Ni–Cu–PGE	Eastern Goldfields	227	✓	✓
Looma 1	Looma	Petroleum	Canning Basin, Broome Platform	171		
FLRD052	Marvel Loch	Au	Yilgarn Craton	164.1		✓
NVCD0102	Marvel Loch	Au	Yilgarn Craton	202		✓
OBGC092	Marvel Loch	Au	Yilgarn Craton	212.8		✓
OBRD067	Marvel Loch	Au	Yilgarn Craton	282.2		✓
UNRD331	Marvel Loch	Au	Yilgarn Craton	80.1		✓
McWhaeRidge	McWhae Ridge		West Kimberley	42.1		
A688	Mesa A	Fe	Pilbara	60.8		✓
MSD4	Minnie Creek	Mo	Gascoyne Province	131.7		✓
MSD5	Minnie Creek	Mo	Gascoyne Province	165.5		✓
MSD6	Minnie Creek	Mo	Gascoyne Province	144.5		✓
MSD7	Minnie Creek	Mo	Gascoyne Province	156		✓
MSD8	Minnie Creek	Mo	Gascoyne Province	168		✓
MSD9	Minnie Creek	Mo	Gascoyne Province	198		✓
MSD1	Minnie Springs	Mo	Gascoyne Province	118		✓
MSD2	Minnie Springs	Mo	Gascoyne Province	272		✓
MSD3	Minnie Springs	Mo	Gascoyne Province	150		✓
MORCD001	Moodini	Au–Cu	Eucla Basin	380.2		✓
MORCD002	Moodini	Au–Cu	Eucla Basin	411.5		✓
AWD003	Nanjilgardy Fault	Au	Capricorn Province (Ashburton)	553.6		✓
EDD005	Nanjilgardy Fault	Au	Capricorn Province (Ashburton)	544		✓
ID001	Nanjilgardy Fault	Au	Capricorn Province (Ashburton)	271.4		✓
LD004	Nanjilgardy Fault	Au	Capricorn Province (Ashburton)	535.7		✓
MD03	Nanjilgardy Fault	Au	Capricorn Province (Ashburton)	201.5		✓
MOD11	Nanjilgardy Fault	Au	Capricorn Province (Ashburton)	359.6		✓
MOD13	Nanjilgardy Fault	Au	Capricorn Province (Ashburton)	58.5		✓
MOD3	Nanjilgardy Fault	Au	Capricorn Province (Ashburton)	288.6		✓
MOD4	Nanjilgardy Fault	Au	Capricorn Province (Ashburton)	190.7		✓
NMOD001	Nanjilgardy Fault	Au	Capricorn Province (Ashburton)	301		✓
NMOD004	Nanjilgardy Fault	Au	Capricorn Province (Ashburton)	398.8		✓
NMOD005	Nanjilgardy Fault	Au	Capricorn Province (Ashburton)	450.6		✓
SPD001	Nanjilgardy Fault	Au	Capricorn Province (Ashburton)	724.2		✓

Appendix 1. continued

Hole name	*Project*	*Commodity*	*Location*	*Total (m)*	*EIS*	*TIR*
PDU2217	Paulsens Gold Mine	Au	Capricorn Province (Ashburton)	56.1		✓
Perindi 1	Perindi	Petroleum	Canning Basin, Pender Terrace	7.6		
PDP1	Pilbara Drilling		Pilbara Craton	104		
PDP2A	Pilbara Drilling		Pilbara Craton, North Pole Dome	50.6		
PDP2B	Pilbara Drilling		Pilbara Craton, North Pole Dome	17.5		
PDP2C	Pilbara Drilling		Pilbara Craton, North Pole Dome	45.3		
09DKRCD002	Quinns	Pb–Zn	Murchison Terrane	291	✓	
09FKRCD001	Quinns	Pb–Zn	Murchison Terrane	228.2	✓	✓
09HBRCD001	Quinns	Pb–Zn	Murchison Terrane	328.2	✓	✓
10TJD001	Quinns	Pb–Zn	Murchison Terrane	340	✓	
09DKRCD001A	Quinns	Pb–Zn	Murchison Terrane	279.4	✓	
09ATD015	Quinns (Austin)	Cu–Zn–Au	Murchison Terrane	305.7		
09ATD019	Quinns (Austin)	Cu–Zn–Au	Murchison Terrane	154.3		
09ATD025	Quinns (Austin)	Cu–Zn–Au	Murchison Terrane	150.4		
09RTD001	Quinns (Austin)	Cu–Zn–Au	Murchison Terrane	248.1		
SFRD0017	Ram Well anomaly	Ni–Cu–PGE	Murchison Terrane	241.1	✓	✓
RKD005	Rocklea Dome	Fe	Pilbara, Rocklea Dome	30.8	✓	
Sally May 2	Sally May	Petroleum	Canning Basin, Broome Platform	494		
SGD001	Salmon Gums	Au	Albany–Fraser Orogen	156	✓	✓
SGD002	Salmon Gums	Au	Albany–Fraser Orogen	228	✓	✓
SGD003	Salmon Gums	Au	Albany–Fraser Orogen	176	✓	✓
SGD004	Salmon Gums	Au	Albany–Fraser Orogen	141	✓	✓
SGD005	Salmon Gums	Au	Albany–Fraser Orogen	210.5	✓	✓
RDH 01	Sammy Webb	Cu, Au, Ag	Centralian Superbasin, Amadeus Basin	515.39	✓	
Santalum 1A	Santalum 1A	Petroleum	Canning Basin, Broome Platform	376.4		
11SAVD003	Savory (SAV08)	Ni–Cu–PGE	Officer Basin	564.7	✓	✓
SHD001A	Shelby	Cu–Au	Capricorn Province	1388.5	✓	✓
Solanum 1	Solanum	Petroleum	Canning Basin, Barbwire Terrace	827.65		
SDH0806	Speewah	V–Ti–PGE	Kimberley	450.4		✓
SDH0901	Speewah	V–Ti–PGE	Kimberley	576.8	✓	✓
SDH0906	Speewah	V–Ti–PGE	Kimberley	168.8	✓	✓
SDH0909	Speewah	Au–fluorite	Kimberley	265.4	✓	
SDH0802	Speewah	V–Ti–PGE	Kimberley	507.2	✓	✓
SDH1001	Speewah	Au–fluorite	Kimberley	522.1	✓	✓
SDH1002	Speewah	Au–fluorite	Kimberley	326.6	✓	✓

Appendix 1. continued

Hole name	*Project*	*Commodity*	*Location*	*Total (m)*	*EIS*	*TIR*
SDH1003	Speewah	Au–fluorite	Kimberley	475.5	✓	✓
SDH1004	Speewah	Au–fluorite	Kimberley	303.3	✓	✓
SDH1005	Speewah	Au–fluorite	Kimberley	300	✓	✓
SDH1006	Speewah	Au–fluorite	Kimberley	473.5	✓	✓
SDH1101	Speewah	Au–fluorite	Kimberley	747.2	✓	✓
SDH1102	Speewah	Au–fluorite	Kimberley	691.6	✓	✓
SDH1103	Speewah	Au–fluorite	Kimberley	729.3	✓	✓
SDH1104	Speewah	Au–fluorite	Kimberley	709.1	✓	✓
SDH1105	Speewah	Au–fluorite	Kimberley	700	✓	✓
SYMD0013	Symons Hill	Ni–Cu–PGE	Murchison Terrane	309.8	✓	✓
SYMD0014	Symons Hill	Ni–Cu–PGE	Murchison Terrane	285.7	✓	✓
09 THD 028	Table Hill	Mn	Officer Basin	288.9	✓	
09 THD 029	Table Hill	Mn	Officer Basin	305.6	✓	
09 THD 030	Table Hill	Mn	Officer Basin	198.9	✓	
09 THD 031	Table Hill	Mn	Officer Basin	255.8	✓	
09 THD 032	Table Hill	Mn	Officer Basin	309.3	✓	
09 THD 033	Table Hill	Mn	Officer Basin	461.7	✓	
WTB14	Teutonic Bore	Pb–Zn	Yilgarn Craton	115.3		
WTB21	Teutonic Bore	Pb–Zn	Yilgarn Craton	206.2		
WTB22	Teutonic Bore	Pb–Zn	Yilgarn Craton	213.7		
WTB29	Teutonic Bore	Pb–Zn	Yilgarn Craton	278.9		
WTB5	Teutonic Bore	Pb–Zn	Yilgarn Craton	149.9		
WTB55	Teutonic Bore	Pb–Zn	Yilgarn Craton	289		
WTB6	Teutonic Bore	Pb–Zn	Yilgarn Craton	213.5		
WTB60	Teutonic Bore	Pb–Zn	Yilgarn Craton	329		
WTB7	Teutonic Bore	Pb–Zn	Yilgarn Craton	166.2		
WTB79	Teutonic Bore	Pb–Zn	Yilgarn Craton	149.4		
WTB9	Teutonic Bore	Pb–Zn	Yilgarn Craton	192.1		
THD001	Thaduna	Cu–Au–Pb–Zn	Yerrida Basin	936.8	✓	✓
Torosa-1	Torosa	Petroleum	Browse Basin	20		✓
Triodia 1	Triodia	Petroleum	Canning Basin, Barbwire Terrace	492		
Turtle 1	Turtle	Petroleum	North Bonaparte Basin	101.7		
UEC05	Ulysses East	Au	Murchison Terrane	111.9	✓	✓
UEC06	Ulysses East	Au	Murchison Terrane	55.1	✓	✓
UEC07	Ulysses East	Au	Murchison Terrane	132.5	✓	✓

Appendix 1. continued

Hole name	*Project*	*Commodity*	*Location*	*Total (m)*	*EIS*	*TIR*
UEC08	Ulysses East	Au	Murchison Terrane	175.2	✓	✓
UEC09	Ulysses East	Au	Murchison Terrane	138.8	✓	✓
WadeKnoll	Wade Knoll		West Kimberley	38		
RWD001	Warburton	Cu	Musgrave Complex, Paterson Orogen	336.3	✓	
RWD002	Warburton	Cu	Musgrave Complex, Paterson Orogen	344.1	✓	
95WGD2	Weld Range	Pb–Zn	Murchison Terrane	233		✓
95WGD4	Weld Range	Pb–Zn	Murchison Terrane	357.8		✓
95WGD6	Weld Range	Pb–Zn	Murchison Terrane	229.7		✓
96GVD001	Weld Range	Pb–Zn	Murchison Terrane	262		✓
WPD013	Wheatley (Kingsley)	Pb–Zn	South West Terrane, Yilgarn Craton	128.8		✓
WPD02	Wheatley (Kingsley)	Pb–Zn	South West Terrane, Yilgarn Craton	198.3		✓
WPD03	Wheatley (Kingsley)	Pb–Zn	South West Terrane, Yilgarn Craton	141		✓
WPD04	Wheatley (Kingsley)	Base metals	South West Terrane, Yilgarn Craton	192.6		✓
WPD07	Wheatley (Kingsley)	Base metals	South West Terrane, Yilgarn Craton	187.7		✓
Wilson Cliffs 1	Wilson Cliffs	Petroleum	Canning Basin, Kidson Sub-basin	28.9		✓
MNDD0001	Windimurra	V–Fe	Murchison Terrane	610.4		✓
MNDD0002	Windimurra	V–Fe	Murchison Terrane	388.3		✓
MNDD0003	Windimurra	V–Fe	Murchison Terrane	574.8		
MNDD0004	Windimurra	V–Fe	Murchison Terrane	480.5		
10CHD006	Yagahong	Cu–Au	Murchison Terrane	195.4	✓	✓
10LAD009	Yagahong	Cu–Au	Murchison Terrane	247	✓	✓
YGDD002	Yalgoo–Bilberatha	Fe	Murchison Terrane	166.7		
12DHDD0001	Yamarna (Dorothy Hills)	Au	Yilgarn Craton	334.5	✓	✓
12DHDD0002	Yamarna (Dorothy Hills)	Au	Yilgarn Craton	351.2	✓	✓
TDH9	Yelma dolomities	Pb–Zn	Earaheedy Basin	138.2		✓
EPT057	Yeneena	Zn–Cu	Paterson Province	420.8	✓	
EPT058	Yeneena	Zn–Cu	Paterson Province	192.6	✓	
EPT060	Yeneena	Zn–Cu	Paterson Province	125.3	✓	
EPT062	Yeneena	Zn–Cu	Paterson Province	229.9	✓	
EPT 0798	Yeneena	Cu–Zn	Paterson Province	401.3	✓	✓
EPT 1174	Yeneena	Cu–Zn	Paterson Province	433.9	✓	✓
YD 10-01	Yuinmery	Pb–Zn	Murchison Terrane	353.6		✓
YD09-01	Yuinmery	Pb–Zn	Murchison Terrane	87.7		✓
YD09-03	Yuinmery	Pb–Zn	Murchison Terrane	389.2		✓
YRC09-01D	Yuinmery	Pb–Zn	Murchison Terrane	103.4		✓
YRC10-13D	Yuinmery	Pb–Zn	Murchison Terrane	338		✓

RECORD 2013/3

HYLOGGER-3: IMPLICATIONS OF ADDING THERMAL-INFRARED SENSING

HANCOCK ET AL.

This Record is published in digital format (PDF) and is available as a free download from the DMP website at <www.dmp.wa.gov.au/GSWApublications>.

Further details of geological products produced by the Geological Survey of Western Australia can be obtained by contacting:

Information Centre
Department of Mines and Petroleum
100 Plain Street
EAST PERTH WESTERN AUSTRALIA 6004
Phone: (08) 9222 3459 Fax: (08) 9222 3444
www.dmp.wa.gov.au/GSWApublications